LPA_3 receptors have orthosteric and allosteric binding sites evidenced under docking studies.

One-sentence summary: Orthosteric and allosteric agonist binding sites in LPA_3 receptors

K. Helivier Solís[1], M. Teresa Romero-Ávila[1], Ruth Rincón-Heredia[1], José Correa-Basurto[2], and J. Adolfo García-Sáinz[1]*

[1]Departamento de Biología Celular y Desarrollo and Unidad de Imagenología, Instituto de Fisiología Celular, Universidad Nacional Autónoma de México. Ciudad Universitaria. Ap. Postal 70-600, Ciudad de México 04510. México

[2] Laboratorio de Diseño y Desarrollo de Nuevos Fármacos e Innovación Biotecnológica, Escuela Superior de Medicina, Instituto Politécnico Nacional. Plan de San Luis y Díaz Mirón S/N, Casco de Santo Tomas, Miguel Hidalgo, Ciudad de México11340, México.

*Correspondence should be addressed to:
J. A. García-Sáinz
Inst. Fisiología Celular, UNAM
Ciudad Universitaria, Ap. Postal 70-600
Ciudad de México 04510
México
Email: agarcia@ifc.unam.mx

Abstract

Comparative studies using LPA and the synthetic ligand, oleoyl-methoxy glycerophosphothionate, OMPT, in cells expressing the LPA_3 receptor revealed differences in these agonists' action. We observed that the latter agonist exhibits two very different potency values, one in the order of 1-10 nm and the other with 30-100-fold less potency and biased pharmacodynamic behavior. The possibility that more than one site might exist for this ligand in the LPA_3 receptor was considered. We performed comparative LPA and OMPT docking studies to obtain structural tridimensional details to achieve binding analysis exploring the whole protein. Our study includes blind docking using the unrefined and refined proteins subjected to hot spot predictions, which allowed us to detect that the LPA binding site is preferentially located in the cytoplasmic (orthosteric site) region. In contrast, OMPT displayed an affinity for an additional binding site (allosteric) located in transmembrane and extracellular regions.

Docking studies also focused on the alpha carbons from Trp102 and Tyr293, founded as the centers for the hot spot predictions. Docking targeted to Trp102 favored binding both ligands in the transmembrane and extracellular regions. In contrast, docking targeted to Tyr293 also shared interaction sites for both ligands but in the cytoplasmic region. These data suggest that OMPT might exhibit a biotypic behavior, promoting different structural rearrangements, which could explain the observed biased behavior.

Keywords: Lysophosphatidic acid; LPA; LPA_3 receptor; oleoyl-methoxy glycerophosphothionate**;** OMPT; biased agonism; byotypic, ligand docking.

1. Introduction

Lysophosphatidic acid (LPA) is a bioactive lipid that exerts many of its actions through six G protein-coupled receptors (GPCRs) of the A family, constituting the LPA subfamily (*1, 2*). Among them is the receptor for LPA_3, which mainly couples to $G_{\alpha i/o}$ and $G_{\alpha q/11}$, participating in diverse signaling events and many physiological and pathophysiological actions (*3, 4*). Structurally, the LPA_3 receptor consists of 7 transmembrane domains, three intracellular loops, and three extracellular loops, with an extracellular amino and an intracellular carboxyl terminus (*3, 4*). Although the LPA_3 receptor has a similarity of approximately 53% with the LPA1 (*5-9*), it has not been crystallized yet, and several domains that regulate the LPA_1 are not conserved in the LPA_3, including the dileucine motif, a mono ubiquitination residue, and a PDZ pattern, among others (*4, 10*). Structural analysis of the LPA_3 receptor showed it conserves motifs/domains typical of the A family of GPCRs, which promote ligand recognition in the binding pocket and include the CWxP, EHR, PIF, and NPxxY domains, each having a specific function during and after agonist attachment (*8, 10-12*). It is generally accepted that ligand binding to the receptor's recognition cavity is flexible, promoting conformational changes that impact its spatial conformation. These dynamic events allow displacements of the intracellular loops and the transmembrane regions, which promote G-protein recruitment and expose sites that can be phosphorylated by GRKs (G protein-coupled receptor kinases) and protein kinases activated by second messengers (*11-14*), thus favoring β-arrestin-receptor interaction, ultimately triggering signaling events (*15-17*). Therefore, determining how a ligand interacts with the receptor provides a fundamental tool for searching for drugs that could effectively regulate its activity and identify the participating mechanisms. In this sense, molecular docking simulations have become a method that allows a better knowledge of the receptor regions in which the ligand could bind, indicating the possible residues involved (*18*).

Pioneer structural work with the LPA_3 receptor has identified residues that interact with the polar head of LPA (*19*). When they are mutated, particularly those in the transmembrane domains 3, 4, 5, and 7, receptor function is altered; these include the sites Arg105 (3.28), Gln106 (3.29), Arg209 (5.38), Lys296 (7.35) and Trp153 (4.64) (in parentheses are the Ballesteros and Weinstein (*20*) numbering scheme, as reported (*21*) (server:

https://gpcrdb.org/protein/lpar3_human/)). The residues Lys296 (7.35) and Trp153 (4.64) directly impact LPA binding and activation of the LPA_3 receptor, decreasing LPA potency and efficacy in RH7777 cells transfected with this receptor subtype (*19*).

No specific agonist for LPA_3 is currently available since most of those ready for use have activity also on the LPA_1 and LPA_2 receptors. A ligand that shows high potency for LPA_3 is 1-oleoyl-2-methyl-sn-glycero-3-phosphothionate (OMPT)(*22*). A recent study (accompanying manuscript) observed that LPA and OMPT exhibit marked pharmacodynamic differences. In particular, two findings were astonishing: firstly, OMPT exerts its effects within two very distinct concentration ranges, and secondly, LPA induced a "receptor refractory state" that blocks the response to rechallenging with the natural agonist; in contrast, OMPT was able to produce a conspicuous response in the presence of LPA (accompanying manuscript). These data again suggest the possibility that two binding sites for these agonists might exist in the LPA_3 receptor, one showing a very high affinity for OMPT (in the 1-10 nM range) and another, likely shared by LPA and OMPT (structural analogs) with a lower affinity in the range of 100-300 nM. Furthermore, a ligand-receptor docking study was achieved to get insights regarding the protein binding site. This docking study and the hot spot predictions indicate the presence of such two sites that might explain the observed functional responses of OMPT. This report is the first that indicates the presence of such two sites, which, in our opinion, opens many further experimental possibilities and helps the understanding of LPA receptor-agonist action, which might aid the development of new agonists and antagonists of potential therapeutic use.

2. Results

To determine the binding parameters (free energy values (ΔG), Kd, and residue interaction) of the LPA_3 receptor agonists, LPA and OMPT, the unrefined 3D model from the Swiss Model program was employed (a 126 $Å^3$ grid box centered on the protein with (x, y, and z) coordinates in grid center for LPA: 6.014, -0.124, and -2.385, and for OMPT: 6.014, -0.124, and -2.385 were used). Molecular docking simulation showed that the LPA_3 receptor binding sites for LPA and

OMPT were different (Table 2), and the binding energy value was lower for OMPT than for LPA.

LPA_3 receptor model without refinement. LPA (blue) reaches the orthosteric site of the LPA_3 receptor with residues preferentially located in intracellular loop 2 and intracellular loop 3, very close to the cytoplasm (Fig. 2). In contrast, OMPT (red) interacted with amino acids located in the extracellular loops 1, 2 and the transmembrane regions 2 and 7 (Fig 2). The 2D scheme shows the LPA-interacting residues (blue) and OMPT-interacting amino acids (red) (Fig. 3). It can be further observed the remarkably different distribution of such binding sites. As depicted in Fig. 4, LPA interacted with Leu220, Thr217, Arg230, Lys216, Val213, Met134, Ile131, Arg135, Pro234, Asn139, Val136, and His137 (Table 2). LPA makes hydrogen bonds with Val136 and His137 π-Alkyl bonds with Arg230, Ile131, Val213, Prol 234, Leu 220, Lys 216, and Met134, which seem to play a crucial role in the ligand recognition by the protein. LPA also interacts with the receptor through Van der Waals forces with Tyr212, Arg135, Asn139, Arg231, and Thr217. Fig. 5 depicts the non-bond interactions of OMPT with the following LPA_3 receptor residues: Leu86, Leu283, Leu279, Leu280, Lys275, Val33, Val36, Thr90, Trp25, Arg276, and Trp277 (Table 2). Similarly, OMPT makes hydrogen bonds with Arg276 and Thr90 and π-sigma interactions with Val33 and Val32. Interestingly, a π-sulfur bonding with Trp25 was also detected, which could be involved in charge transfer and might help to intercalate the compound within the receptor's binding site. Furthermore, OMPT promotes π-Alky and Alkyl interaction with Leu280, Val33, Leu283, Trp277, and Val32.

LPA_3 refined Model. LPA (Fig. 6; blue) interacts with the receptor in the intracellular Loop 2 and intracellular Loop 3, which, like in the LPA_3 unrefined model, was very close to the cytoplasm. Docking of OMPT (Fig. 6; red) interacted with the receptor amino acids located in transmembrane regions 5, 6, 7, and 8 as well as the extracellular loop 3 (Fig. 6). The 2D scheme shows the LPA-interacting residues (Fig. 7; blue) and the OMPT-interacting amino acids (red). Again, the markedly different distribution of such binding sites can be observed. Our results showed in the 2D maps that LPA interacts with receptor residues including Leu220, Arg230, Val219, Lys216, Thr217, Arg135, Val136, Met134, Ile131, Pro234, Val213, Thr217 (Table 3). It is noteworthy that the polar head of LPA forms hydrogen bonds with Val136 and Met134, as

well as π-Alkyl and Alkyl interactions with residues Arg23, Lys216, Pro234, Ile131, Val213, Leu220, and Val219, which might stabilize the ligand-receptor interaction. Likewise, LPA has Van der Waals interactions with Arg231, Thr217, Tyr212 and His 137 and Arg135 (Fig. 8). The LPA_3-OMPT 2D map showed that this ligand forms hydrogen bonds with Arg105 and Trh90, as well as Alkyl and P-Alkyl interactions with residues Leu259, Trp191, Leu113, Trp252, Val258, Leu179, Leu279, Lys275 and Ala282 (Fig. 9), suggesting that they participate in receptor-ligand recognition. Similarly, Van der Waals forces participate in the ligand-receptor recognition at residues Ala180, Leu109, Gln106, Leu86, Val33, Trp25, Arg276, Trp14, Leu256, Asp110, Gly 255, and Phe278 (Table 3).

Trp102-focused model. Trp102-focused docking was performed for LPA and OMPT. Interestingly, LPA (Fig. 10, blue) interacts with the receptor in sites located mainly in transmembrane regions 1, 2, and 7 and with the extracellular loops 1, 2, and 3, which is in complete contrast with what was observed in the unfocused analyses (i.e., refined and unrefined). OMPT (Fig. 10; red) interacts with almost the same amino acids observed in the unfocused analysis (Figs. 2 and 6). It is worth noticing that the receptor-agonist interactions were very close, indicating that under this analysis conditions, both ligands interact with some of the allosteric critical sites but also involve ligand-selective additional ones. The 2D map shows the residues at which LPA and OMPT interact with the receptor, showing in orange the residues that are shared between the two ligands with the receptor, while in blue are those that interact with LPA, while in red are the residues that interact only with OMPT (Fig. 11). The 2D map showed that most amino acids interacting with the agonists are shared. However, the interactions that form are not the same due to their chemical differences. For instance, LPA interacted with the amino acids Leu283, Leu280, Leu279, Met87, Val33, Thr90, Trp25, Arg276, Lys29 (Table 4), in which Arg276 and Lys29 form hydrogen bonds mainly in the polar head of LPA, Alkyl and π-Alkyl interactions were also determined with the amino acids Leu279, Val33, Leu213, Leu86, Met87, Leu280 and Trp25, which could be favoring the interaction of the ligand with the receptor (Fig. 12). In contrast, the amino acids Thr90, Gly37, Tyr83, ASp23, Lys275, and Trp272 associate via Van der Waals forces with the ligand. OMPT-interacting amino acids and ΔG values are presented in Table 4. These docking simulations indicated that OMPT did not form hydrogen bridges with the receptor, prevailing the Alkyl and π-Alkyl interactions between

residues Leu279, Val33, Met87, Leu86, Tyr83, Leu283, Leu280 and Leu279, While Trp25, Trp277, Ile32, Val36, Thr90 and Gly37 interact with the receptor by Van der Waals forces, which would favor receptor binding (Fig. 13).

Tyr293-focused model. Fig. 14 shows the non-bond interaction of LPA (blue) and OMPT (red) with the LPA_3 receptor when the docking analysis is focused on Tyr293. In this docking simulation, the LPA binding sites were remarkably similar to what was observed in the unrefined and refined analyses (Figs. 2 and 6), i.e., interaction occurred with the intracellular loops 1, 2, and 3 near the cytoplasm. The 2D scheme (Fig. 15) shows the amino acid residues in which both ligands, LPA and OMPT, interact (orange) (Fig. 15). The 2D map shows that LPA binds to Leu220, Lys216, Thr217, Ile131, Val213, Pro234, Arg135, Met134, Val136, Asn139, His137, Phe63 (Table 5). Residues Asn139, Ser138, Val136, and His137 form hydrogen bridges with the polar head of LPA, likely favoring the interaction of the ligand with the receptor (Fig. 16). Residues Pro234, Val213, Lys216, Ile131, Met134, and Leu220 form alkyl bonds, and Tyr212, Arg231, Arg135, Phe63, Thr217, and Arg230 promote interaction with the receptor through Van der Waals forces; both interactions could favor the interaction and stability of the ligand with the receptor (Fig. 17). The 2D map shows that OMPT binds to residues Arg230, Leu220, Lys216, Thr217, Arg231, Ile131, His137, Val136, Thr233, Pro234 (Table 5). It is remarkable that, in this case, both ligands interact with essentially the same amino acids and employ the same type of association observed for LPA in the unrefined and refined docking analysis (Figs. 2, 6, and 14). Arg135 did not seem to interact with OMPT (Fig. 17).

3. Discussion

The present work was designed to define if LPA and OMPT bind to a single site or if different agonist recognition cavities exist in the LPA_3 receptor. The possible existence of more than one coupling region was suggested in experiments using cultured cells (accompanying manuscript). Blind docking studies were performed using the predicted structure of LPA_3 (UniProt sequence). Unrefined, refined, and focused (to Tyr293 and Trp102) docking analyses were carried out. As

indicated, T293 was identified as a critical amino acid for binding the LPA antagonist, Ki16425, and an extensive series of agents interacting with the LPA_3 receptor (*23*). Trp102 was consistently detected in the hot spot prediction and confirmed by docking analysis; therefore, a docking study focused on this residue was also performed.

Previous research by Valentine et al. (*19*), also using docking/ computational modeling, identified that the LPA_3 receptor interacted mainly with the polar head of LPA at Arg105 (3.28), Glu106 (3.29), Trp153 (4.50, reported as 4.64), Arg209 (5.60, reported as 5.38), Arg276 (7.36) and Lys275 (7.35, reported as 7.36). These sites were considered critical for LPA binding to the receptor; mutation of these residues affected the function of the LPA_3 receptors, as reflected by decreased agonist efficacy and potency. As expected, such modifications eliminated ionic interactions in the modeled LPA_3-ligand prototype(*19*). The site identified by these authors is located near the extracellular surface of the receptor, i.e., with some proximity to the allosteric OMPT region detected in the present work. Among these residues are Lys 275 and Arg276 in the unrefined docking; in the refined analysis, some OMPT sites are shared with those reported by Valentine et al. (*19*) for LPA; they include Arg105, Gln106, Lys275, and Arg276 (i.e., a similarity of 66.6 % of the residues). When our Try102-focused docking was compared, only Arg276 (binding site shared in this analysis by LPA and OMPT) coincided with the data previously reported (*19*). There was no correspondence in the Tyr293-focussed docking analysis. The reasons for the discrepancies detected are currently unknown, but they can be attributed to using an unbiased approach in our case. In contrast, the similarity to the Sphingosine 1-phosphate type 1 receptor was employed in the computational homology modeling applied by the other group (*19*). Furthermore, the analysis tools have since evolved considerably; the previous work (*19*) was performed more than 15 years ago. To our knowledge, no other docking study on the LPA_3 receptor has been reported. Crystallographic analysis will solve these discrepancies and it would be of great help to achieve further advances.

Our findings suggest that the LPA_3 receptor has two distinct agonist binding sites that are original for this receptor, but many other GPCRs exhibit several ligand recognition cavities. This aspect has been reviewed, observing that many GPCRs have a coupling region for the natural agonists, which is frequently referred to as the orthosteric binding site (as used in this

manuscript), but that other recognition cavities also exist, defined as allosteric sites; these two types of regions generally do not overlap and are frequently spatially located in distinct structural domains (*24, 25*). Based on the docking studies, we determined that the LPA_3 receptor has a binding site for LPA (orthosteric) and another for OMPT (allosteric). In the blind and refined dockings, the Kd value observed suggested higher affinities for OMPT than for LPA, which is similar to what we observed in the in cellulo experiments (accompanying manuscript).

The docking results in the unrefined and refined protein showed that LPA had a lower binding affinity (ΔG) to the orthosteric site than OMPT to the allosteric region. This finding is consistent with the observation that most OMPT effects (accompanying manuscript), including receptor phosphorylation and ERK activation, occur at much lower concentrations than those induced by LPA. Interestingly, LPA was more potent and effective than OMPT in increasing intracellular calcium, raising the possibility that the activity of OMPT could involve interaction not only with the allosteric but also with the orthosteric site (accompanying manuscript).

The 2D structure of the LPA_3-LPA conformer showed that the receptor accommodates LPA by its polar head (phosphate group). However, differences were observed in the residues involved in the unrefined and refined docking analyses; for example, in the refined docking analysis, Met134 and Val136 formed hydrogen bonds with the phosphate group of LPA, whereas in the unrefined docking analysis, such interactions involved Val136 and His137.

The LPA_3-OMPT conformer showed that the binding with the polar head (phosphothionate) mainly involved two hydrogen bonds with Thr90 and Arg276 in the unrefined analysis, while for the refined docking study, Tht90 and Arg105 (but not Arg276) interacted with the oxygen atoms of the phosphothionate group.

Interestingly, ligand-binding residues in the refined and unrefined protein docking analyses shared 79% of the amino acids; i.e., both docking studies were consistent. It is noteworthy that the focused analyses “displace” the binding of the agonists in such a way that in the Trp102-focused examination, both ligands bind to the allosteric cavity (site plus surroundings), and in the

Tyr293-focussed studies, the vice-versa took place, i.e., both ligands interact with the orthosteric cavity.

The main conclusion of our study is that the blind docking simulations, with the refined and unrefined approaches, show that the LPA_3 receptor has an orthosteric binding site for LPA and an additional allosteric binding pocket to which OMPT couples with high affinity. Allosteric ligands are usually divided into positive, negative, and neutral based on their ability to enhance, diminish, or not modify the effect of the natural agonist; interestingly, neutral allosteric molecules can exert an effect by themselves (*26-28*). It is conceivable that the ligand interaction with the two distinct binding pockets in LPA_3 might promote various conformational changes in transmembrane regions (such as 6 and 7) or helix 8, which have already been observed for other family A GPCRs, to which LPA_3 belongs. The present findings open new research possibilities to explore the binding sites and the effects of distinct ligands that interact with the LPA_3 receptor, which is particularly important considering the physiological and physiopathological events in which it is involved(*3, 4*).

4. Methods

4.1 Modeling of LPA_3 receptor structure, Gene ID:23566

The LPA_3 has not yet been crystallized. Therefore, we were forced to predict its most likely 3D structure. Prediction of this structure was based on the amino acid sequence obtained from the Uniprot database using the Q9UBY5 entry (https://www.uniprot.org/uniprotkb/Q9UBY5/entry). Three of the most frequently utilized servers for structure prediction were employed: SWISS-MODEL (https://swissmodel.expasy.org/), I-TASSER (https://zhanggroup.org/I-TASSER/), and AlphaFold database (https://alphafold.ebi.ac.uk/). Table 1 enlists the values obtained using these servers and programs.

Subsequently, protein sequences from the three models generated and that used from UniProt were subjected to sequence alignments employing the PROMALS3D server (Fig. 1; http://prodata.swmed.edu/promals3d/promals3d.php) to determine the gaps or residue insertions

that improve the alignment identity with the 3D protein templates during the protein folding. Although the data obtained showed that the 3D structure built with AlphaFold was the best evaluated structurally, the alignment showed that several mutations or deletions improved the 3D structure quality, possibly eliminating residues that can interact with the ligands. Therefore, the Swiss model was preferred because the best values were estimated by ERRAT and a second evaluation of Ramachandran maps; additionally, the sequence obtained was identical to the UniProt Q9UBY5 entry.

42.2 Refined and validation of the LPA_3 receptor 3D structure.

A protein 3D structure refinement was carried out to perform accurate docking simulations. The model obtained from the Swiss Model server was subjected to molecular refinement using ReFOLD (https://www.reading.ac.uk/bioinf/ReFOLD/ReFOLD3_form.html). The refined protein with the best score was used for the docking study to explore receptor cavities capable of ligand recognition.

4.3 Search for ligand binding sites on the LPA_3 receptor

Additionally, the hot spot prediction was performed to identify possible ligand recognition cavities using the BetaCavityWeb (http://voronoi.hanyang.ac.kr/betacavityweb/) and the Fpocketweb (http://durrantlab.com/fpocketweb) servers. The protein from the Swiss Model server, as well as that from ReFOLD, were used. Both servers calculate these cavities for a given molecular structure and a defined spherical probe and report their geometrical properties, such as volume, boundary area, buried area, and other parameters described on their websites. In both proteins, cavities or channels in the protein can be predicted mainly at the barrel end built by an alpha secondary structure, a pattern observed in the refined and unrefined protein.

4.4 Docking of the ligands, LPA and OMPT, at the LPA_3 receptor binding sites

The 3D structures of the ligands studied were obtained from PubChem (ID 5497152 for LPA and ID 16078994 for OMPT), and their molecular structure minimization was carried out using the

Avogadro program (https://avogadro.cc/docs/tools/auto-optimize-tool/); the lengths and angles of the links and junctions of interatomic as well as their geometry were appropriated and transmitted with the optimized energy.

After ligand structure minimization, a blind docking study of the native protein (unrefined) was performed, allowing us to explore the whole protein. It is worth noticing that it has been reported that Tyr293 participates in the binding of the LPA antagonist, Kil6425, and also of an extensive series of pharmacological agents used in therapeutics(*23*). Residue Trp102 was also particularly interesting because it was consistently found in the hot spot predictions and visualized exposed and centered in a cavity according to 3D structural analysis with PyMol (https://www.pymol.org/). Therefore, a focused docking on the alpha carbon of Tyr293 and Trp102 was also performed. Subsequently, the files of ligands and protein employed to perform the docking analysis were obtained using the program Autodock tools 1.5.6 (ADT) (https://autodocksuite.scripps.edu/adt/). Autogrid4 and Autodock4 programs were used for getting the grid maps and docking results, respectively.

Blind docking simulations consist of adjusting the grid box (search area) to the maximum space allowed by the program, i.e., 126 $Å^3$ and a grid space of 0.375 $Å^3$, centered by default on the proteins. All simulations were performed using the LINUX operating system (Centus) and the Lamarckian genetic algorithm, which was chosen to search for the best ligand conformers coupled to the LPA_3 receptor. This process generates the most probable results of the ligand conformations within the receptor search space, with a maximum number of 1×10^7 energy evaluations and a population of 100 randomized individuals (represented by the 100 best evaluations). For the focused docking, the grid box was 60 $Å^3$ with a grid space of 0.375 $Å^3$centered on the alpha carbons of Tyr293 or Trp102, as mentioned previously. The 2D maps showing the receptor's residues interacting with the ligands were obtained using the Discovery Studio Visualizer (https://discover.3ds.com/discovery-studio-visualizer-download).

References

1. J. W. Choi, D. R. Herr, K. Noguchi, Y. C. Yung, C. W. Lee, T. Mutoh, M. E. Lin, S. T. Teo, K. E. Park, A. N. Mosley, J. Chun, LPA receptors: subtypes and biological actions. *Annu. Rev. Pharmacol. Toxicol.* **50**, 157-186 (2010)10.1146/annurev.pharmtox.010909.105753).
2. Y. C. Yung, N. C. Stoddard, J. Chun, LPA receptor signaling: pharmacology, physiology, and pathophysiology. *J. Lipid Res.* **55**, 1192-1214 (2014); published online EpubMar 18 (10.1194/jlr.R046458).
3. K. Hama, J. Aoki, LPA(3), a unique G protein-coupled receptor for lysophosphatidic acid. *Prog. Lipid Res.* **49**, 335-342 (2010); published online EpubOct (10.1016/j.plipres.2010.03.001).
4. K. H. Solís, M. T. Romero-Ávila, A. Guzmán-Silva, J. A. García-Sáinz, The LPA(3) Receptor: Regulation and Activation of Signaling Pathways. *Int J Mol Sci* **22**, 6704 (2021); published online EpubJun 23 (10.3390/ijms22136704).
5. J. J. Contos, J. Chun, The mouse lp(A3)/Edg7 lysophosphatidic acid receptor gene: genomic structure, chromosomal localization, and expression pattern. *Gene* **267**, 243-253 (2001); published online EpubApr 18 (10.1016/s0378-1119(01)00410-3).
6. J. I. Fells, R. Tsukahara, J. Liu, G. Tigyi, A. L. Parrill, Structure-based drug design identifies novel LPA3 antagonists. *Bioorgan Med Chem* **17**, 7457-7464 (2009); published online EpubNov 1 (10.1016/j.bmc.2009.09.022).
7. N. Fukushima, J. Chun, The LPA receptors. *Prostaglandins Other Lipid Mediat* **64**, 21-32 (2001); published online EpubApr (10.1016/s0090-6980(01)00105-8).
8. Y. C. Yung, N. C. Stoddard, J. Chun, LPA receptor signaling: pharmacology, physiology, and pathophysiology. *J Lipid Res* **55**, 1192-1214 (2014); published online EpubJul (10.1194/jlr.R046458).
9. K. Bandoh, J. Aoki, A. Taira, M. Tsujimoto, H. Arai, K. Inoue, Lysophosphatidic acid (LPA) receptors of the EDG family are differentially activated by LPA species. Structure-activity relationship of cloned LPA receptors. *FEBS Lett.* **478**, 159-165 (2000); published online EpubJul 28 (10.1016/s0014-5793(00)01827-5).
10. N. M. Urs, A. P. Kowalczyk, H. Radhakrishna, Different mechanisms regulate lysophosphatidic acid (LPA)-dependent versus phorbol ester-dependent internalization of the LPA1 receptor. *J. Biol. Chem.* **283**, 5249-5257 (2008); published online EpubFeb 29 (10.1074/jbc.M710003200).
11. T. Flock, A. S. Hauser, N. Lund, D. E. Gloriam, S. Balaji, M. M. Babu, Selectivity determinants of GPCR-G-protein binding. *Nature* **545**, 317-322 (2017); published online EpubMay 18 (10.1038/nature22070).
12. A. S. Hauser, A. J. Kooistra, C. Munk, F. M. Heydenreich, D. B. Veprintsev, M. Bouvier, M. M. Babu, D. E. Gloriam, GPCR activation mechanisms across classes and macro/microscales. *Nat Struct Mol Biol* **28**, 879-888 (2021); published online EpubNov (10.1038/s41594-021-00674-7).
13. D. Hilger, M. Masureel, B. K. Kobilka, Structure and dynamics of GPCR signaling complexes. *Nat Struct Mol Biol* **25**, 4-12 (2018); published online EpubJan (10.1038/s41594-017-0011-7).
14. Q. Zhou, D. Yang, M. Wu, Y. Guo, W. Guo, L. Zhong, X. Cai, A. Dai, W. Jang, E. I. Shakhnovich, Z. J. Liu, R. C. Stevens, N. A. Lambert, M. M. Babu, M. W. Wang, S.

Zhao, Common activation mechanism of class A GPCRs. *Elife* **8**, (2019); published online EpubDec 19 (10.7554/eLife.50279).

15. M. R. Arkin, M. Randal, W. L. DeLano, J. Hyde, T. N. Luong, J. D. Oslob, D. R. Raphael, L. Taylor, J. Wang, R. S. McDowell, J. A. Wells, A. C. Braisted, Binding of small molecules to an adaptive protein-protein interface. *Proc Natl Acad Sci U S A* **100**, 1603-1608 (2003); published online EpubFeb 18 (10.1073/pnas.252756299).
16. A. D. Huber, S. Poudel, Y. Li, W. Lin, J. Wu, D. J. Miller, T. Chen, Ligand flexibility and binding pocket malleability cooperate to allow selective PXR activation by analogs of a promiscuous nuclear receptor ligand. *Structure* **31**, 1545-1555 e1549 (2023); published online EpubDec 7 (10.1016/j.str.2023.08.020).
17. A. Stank, D. B. Kokh, J. C. Fuller, R. C. Wade, Protein Binding Pocket Dynamics. *Acc Chem Res* **49**, 809-815 (2016); published online EpubMay 17 (10.1021/acs.accounts.5b00516).
18. M. Rosell, J. Fernandez-Recio, Docking-based identification of small-molecule binding sites at protein-protein interfaces. *Comput Struct Biotechnol J* **18**, 3750-3761 (2020)10.1016/j.csbj.2020.11.029).
19. W. J. Valentine, J. I. Fells, D. H. Perygin, S. Mujahid, K. Yokoyama, Y. Fujiwara, R. Tsukahara, J. R. Van Brocklyn, A. L. Parrill, G. Tigyi, Subtype-specific residues involved in ligand activation of the endothelial differentiation gene family lysophosphatidic acid receptors. *J. Biol. Chem.* **283**, 12175-12187 (2008); published online EpubMay 2 (10.1074/jbc.M708847200).
20. J. A. Ballesteros, H. Weinstein, Integrated methods for the construction of three-dimensional models and computational probing of structure-function relations in G protein coupled receptors. *Methods Neurosci.* **25**, 366-428 (1995)https://doi.org/10.1016/S1043-9471(05)80049-7).
21. G. Pandy-Szekeres, C. Munk, T. M. Tsonkov, S. Mordalski, K. Harpsoe, A. S. Hauser, A. J. Bojarski, D. E. Gloriam, GPCRdb in 2018: adding GPCR structure models and ligands. *Nucleic Acids Res.* **46**, D440-D446 (2018); published online EpubJan 4 (10.1093/nar/gkx1109).
22. Y. Hasegawa, J. R. Erickson, G. J. Goddard, S. Yu, S. Liu, K. W. Cheng, A. Eder, K. Bandoh, J. Aoki, R. Jarosz, A. D. Schrier, K. R. Lynch, G. B. Mills, X. Fang, Identification of a phosphothionate analogue of lysophosphatidic acid (LPA) as a selective agonist of the LPA3 receptor. *J. Biol. Chem.* **278**, 11962-11969 (2003); published online EpubApr 4 (10.1074/jbc.M209168200).
23. D. S. Malar, K. Verma, M. I. Prasanth, T. Tencomnao, J. M. Brimson, Network analysis-guided drug repurposing strategies targeting LPAR receptor in the interplay of COVID, Alzheimer's, and diabetes. *Sci Rep* **14**, 4328 (2024); published online EpubFeb 21 (10.1038/s41598-024-55013-9).
24. D. Wootten, A. Christopoulos, P. M. Sexton, Emerging paradigms in GPCR allostery: implications for drug discovery. *Nat Rev Drug Discov* **12**, 630-644 (2013); published online EpubAug (10.1038/nrd4052).
25. R. R. Neubig, M. Spedding, T. Kenakin, A. Christopoulos, N. International Union of Pharmacology Committee on Receptor, C. Drug, International Union of Pharmacology Committee on Receptor Nomenclature and Drug Classification. XXXVIII. Update on terms and symbols in quantitative pharmacology. *Pharmacol Rev* **55**, 597-606 (2003); published online EpubDec (10.1124/pr.55.4.4).

26. S. Shen, C. Zhao, C. Wu, S. Sun, Z. Li, W. Yan, Z. Shao, Allosteric modulation of G protein-coupled receptor signaling. *Front Endocrinol (Lausanne)* **14**, 1137604 (2023)10.3389/fendo.2023.1137604).
27. J. J. Liu, R. Horst, V. Katritch, R. C. Stevens, K. Wuthrich, Biased signaling pathways in beta2-adrenergic receptor characterized by 19F-NMR. *Science* **335**, 1106-1110 (2012); published online EpubMar 2 (10.1126/science.1215802).
28. A. E. Wakefield, D. Bajusz, D. Kozakov, G. M. Keseru, S. Vajda, Conservation of Allosteric Ligand Binding Sites in G-Protein Coupled Receptors. *J Chem Inf Model* **62**, 4937-4954 (2022); published online EpubOct 24 (10.1021/acs.jcim.2c00209).

ACKNOWLEDGMENTS

This research was partially supported by Grants from CONAHCYT (Fronteras 6676) and DGAPA (IN201221 and IN201924). We thank Dr. A. César Poot-Hernández for his suggestions to improve the manuscript. The advice and technical support of the following members of the indicated Service Units of our Institute is gratefully acknowledged: Dr. Héctor Malagón and Dr. Claudia Rivera (Bioterio); Juan Barbosa and Gerardo Coello (Cómputo); and Aurey Galván and Manuel Ortínez (Taller). K. Helivier Solís is a student of the Programa de Doctorado en Ciencias Biomédicas (UNAM) of Universidad Nacional Autónoma de México (account 520014983).

CRediT authorship contribution statement

Conceptualization: KHS, JC-B, JAG-S

Methodology: KHS, JC-B

Investigation: KHS, MTR-A, RR-H, JC-B

Visualization: KHS, MTR-A, RR-H, JC-B

Funding acquisition: JAG-S

Writing – original draft: KHS, JC-B, JAG-S

Writing – review & editing: KHS, MTR-A, RR-H, JC-B, JAG-S

CONFLICT OF INTEREST STATEMENT

The authors declare that there is no conflict of interest regarding the publication of this article.

DATA AVAILABILITY STATEMENT

The data are available from the corresponding author upon reasonable request.

Table 1

Structural evaluation of the 3D models generated using the three most frequently used homology modeling servers (in green, the best values).

Server	**MolProbity: Protein Geometry/ Ramachandran favored**	**SAVESv6.0: ERRAT**	**SAVESv6.0: VERIFY**
SWISS-MODEL	91.45%	94.8052	33.14%
I-TASSER	78.92%	83.4302	38.81%
AlphaFold	95.18%	94.3038	29.01%

Table 2.

Blind docking for LPA and OMPT at the LPA_3 receptor with a 126 $Å^3$ grid box centered on the protein.

Ligand	ΔG (kcal/mol)	Kd (nM)	Sites of ligand-receptor interaction
LPA	-3.98	1200	Leu220, Thr217, Arg230, Lys216, Val213, Met134, Ile131, Arg135, Pro234, Asn139, Val136, His137
OMPT	-5.31	128	Leu86, Leu283, Leu279, Leu280, Lys275, Val33, Val36, Thr90, Trp25, Arg276, Trp277

Table 3.

Refined docking for LPA and OMPT at the LPA_3 receptor refined with ReFOLD with a 126 $Å^3$ grid box

Ligand	ΔG (kcal/mol)	Kd (nM)	Interactions
LPA	-5.01	211	Leu220, Arg230, Val219, Lys216, Thr217, Arg135, Val136, Met134, Ile131, Pro234, Val213, Thr217
OMPT	-5.67	70	Trp252, Leu113, Asp110, Trp191, Leu279, Phe278, Gly255, Leu259, Gln106, Leu86, Arg105, Lys275, Leu179, Thr90, Thr25, Arg276

Table 4.

Docking focused on the alpha carbon of residue Trp102 of LPA and OMPT in the REFOLD-refined LPA_3 receptor with a 126 $Å^3$ grid box.

Ligand	**ΔG (kcal/mol)**	**Kd (nM)**	**Interactions**
LPA	-5.99	40	Leu283, Leu280, Leu279, Met87, Val33, Thr90, Trp25, Arg276, Lys29
OMPT	-5.15	167	Leu283, Leu280, Leu279, Tyr83. Val36, Met87, Val33, Thr90, Trp25, Arg276, Trp277, Leu86

Table 5.

Docking focused on the alpha carbon of Tyr293 for LPA and OMPT in the REFOLD-refined LPA3 receptor with a 126 $Å^3$ grid box.

Ligand	**ΔG (kcal/mol)**	**Kd (nM)**	**Interactions**
LPA	-5.79	57	Leu220, Lys216, Thr217, Ile131, Val213, Pro234, Arg135, Met134, Val136, Asn139, His137, Phe63
OMPT	-4.64	396	Arg230, Leu220, Lys216, Thr217, Arg231, Ile131, His137, Val136, Thr233, Pro234

Figure Legends.

Fig. 1. Alignment of the FASTA sequence of the LPA_3 receptor (Q9UBY5) with the 3D model programs I-Tasser (model 01.pdb chainA_s001), Swiss Model (model1) and AlphaFold (AF-A v4).

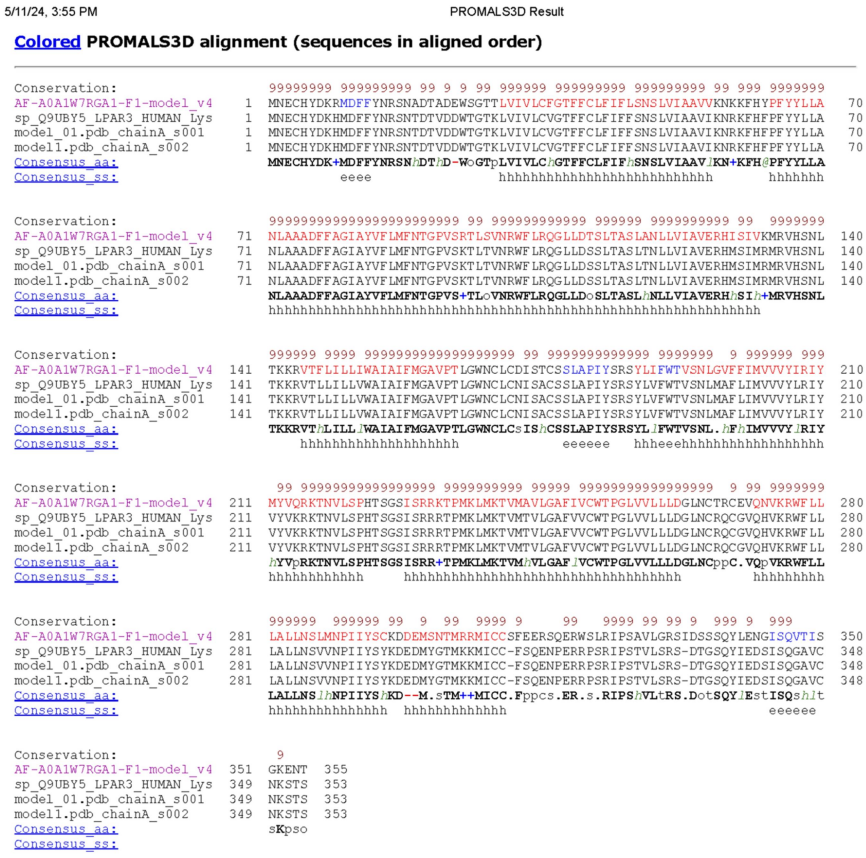

Fig. 2. Images resulting from the LPA_3-LPA (blue) and LPA3-OMPT (red) docking analysis using PyMol.

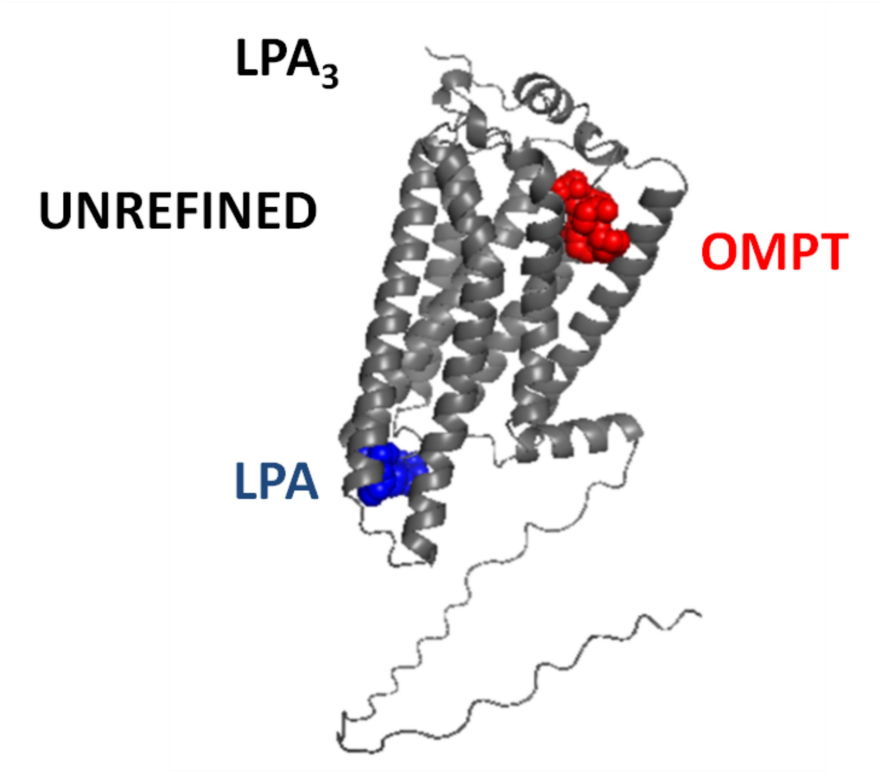

Fig. 3. Graphical representation of LPA (blue) and OMPT (red) binding to the LPA_3 receptor.

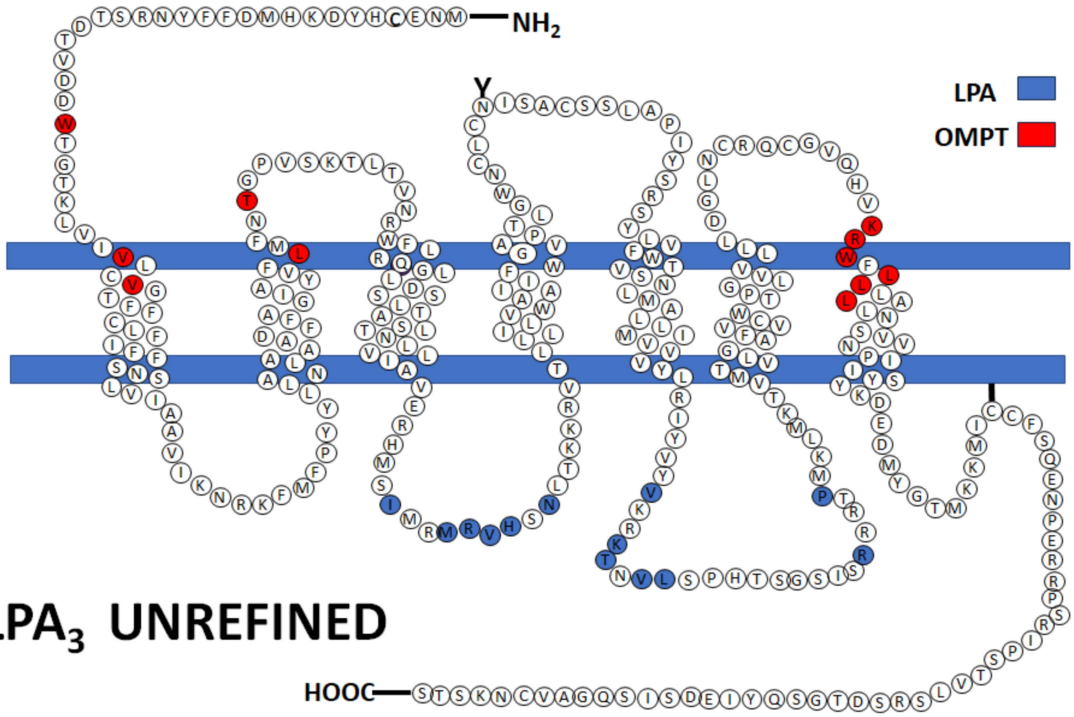

Fig. 4. The 2D diagram shows interactions observed at the LPA_3 binding site with LPA (Discovery Studio Visualizer); critical amino acids contributing to interactions are shown in circles.

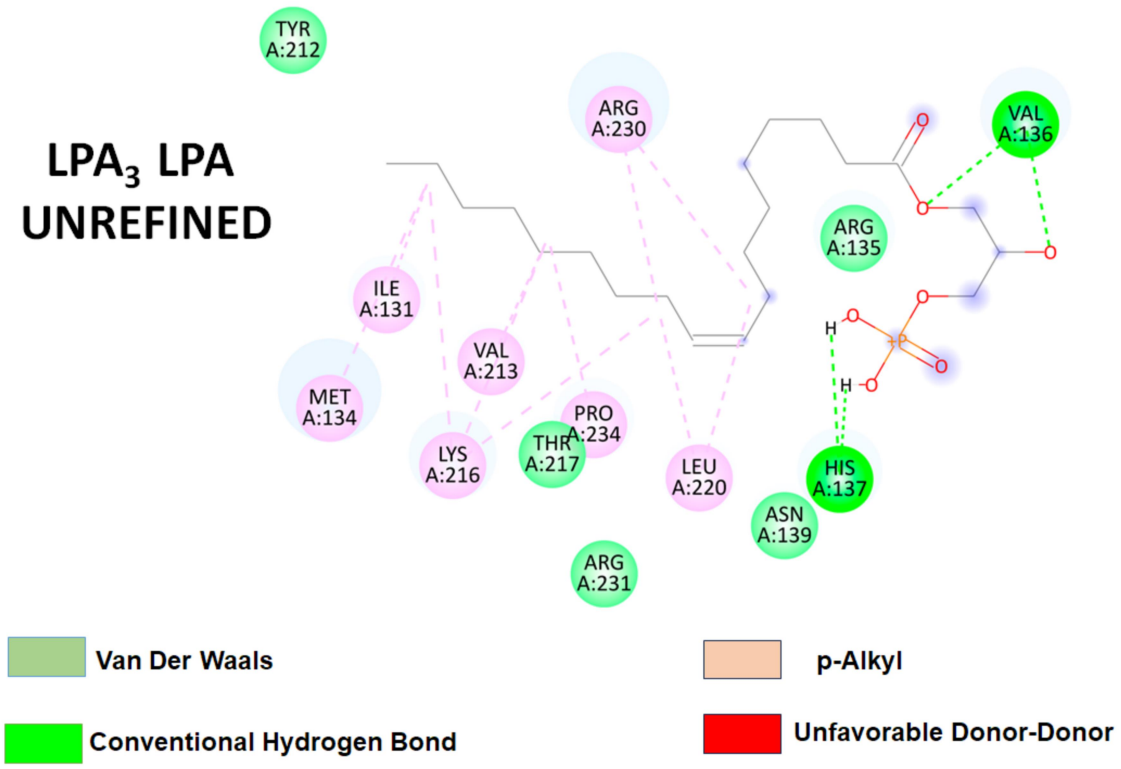

Fig. 5. The 2D diagram shows interactions at the LPA_3 binding site with OMPT (Discovery Studio Visualizer). Critical amino acids contributing to interactions are shown in circles.

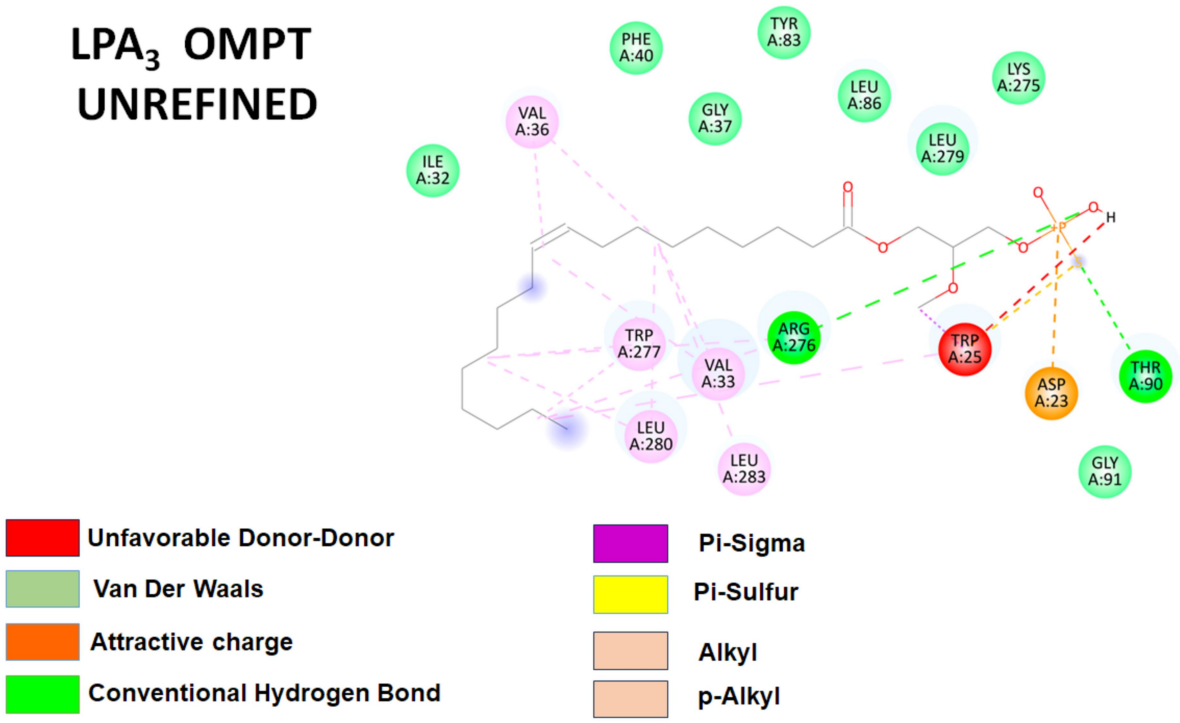

Fig. 6. Images resulting from the LPA_3-LPA (blue) and LPA_3-OMPT (red) docking analysis using PyMol.

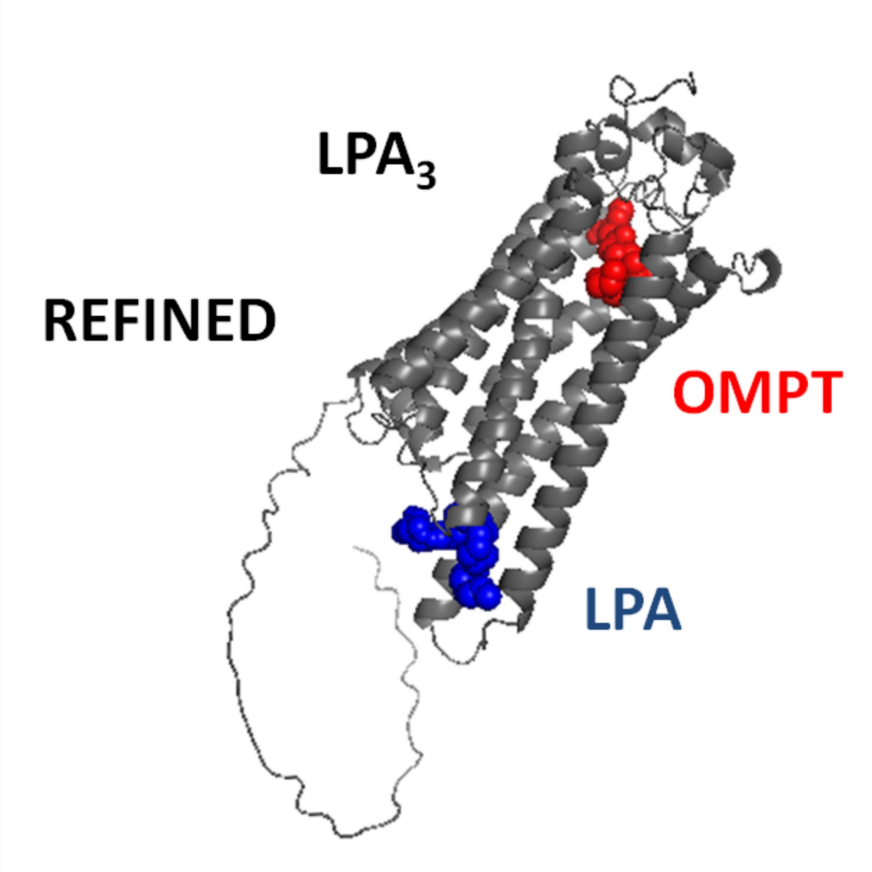

Fig. 7. Graphical representation of LPA (blue) and OMPT (red) binding to the LPA_3 receptor.

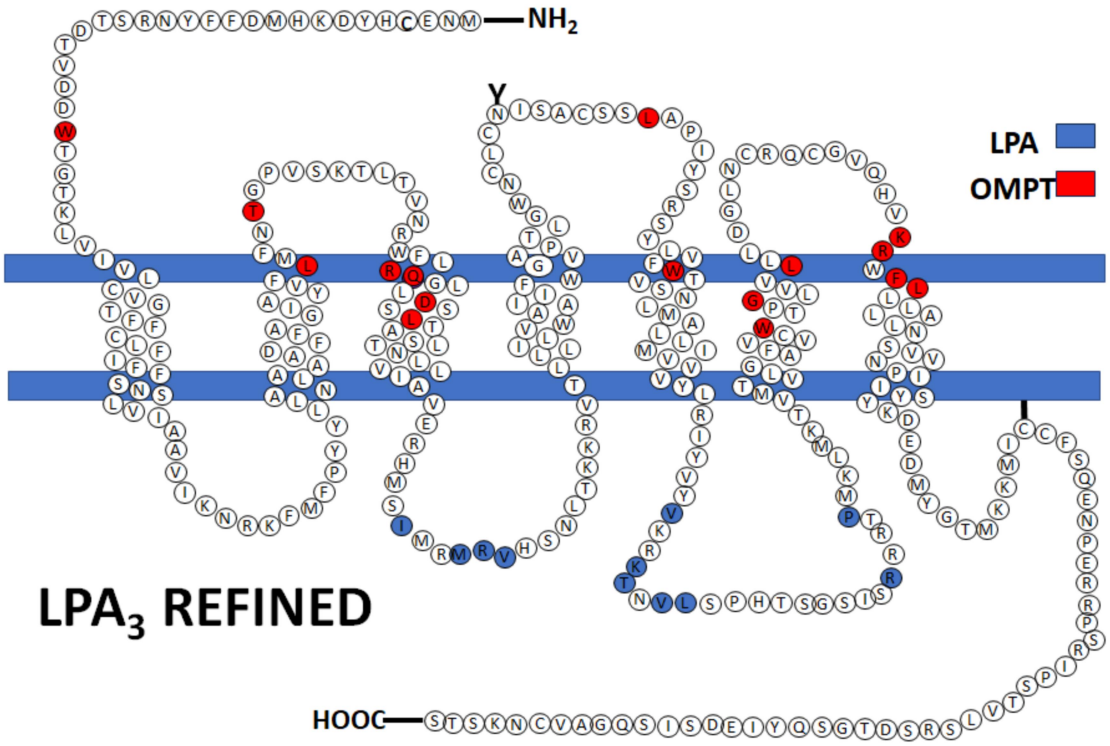

Fig. 8. The 2D diagram shows interactions at the LPA_3 binding site with LPA (Discovery Studio Visualizer). Critical amino acids contributing to interactions are shown in circles.

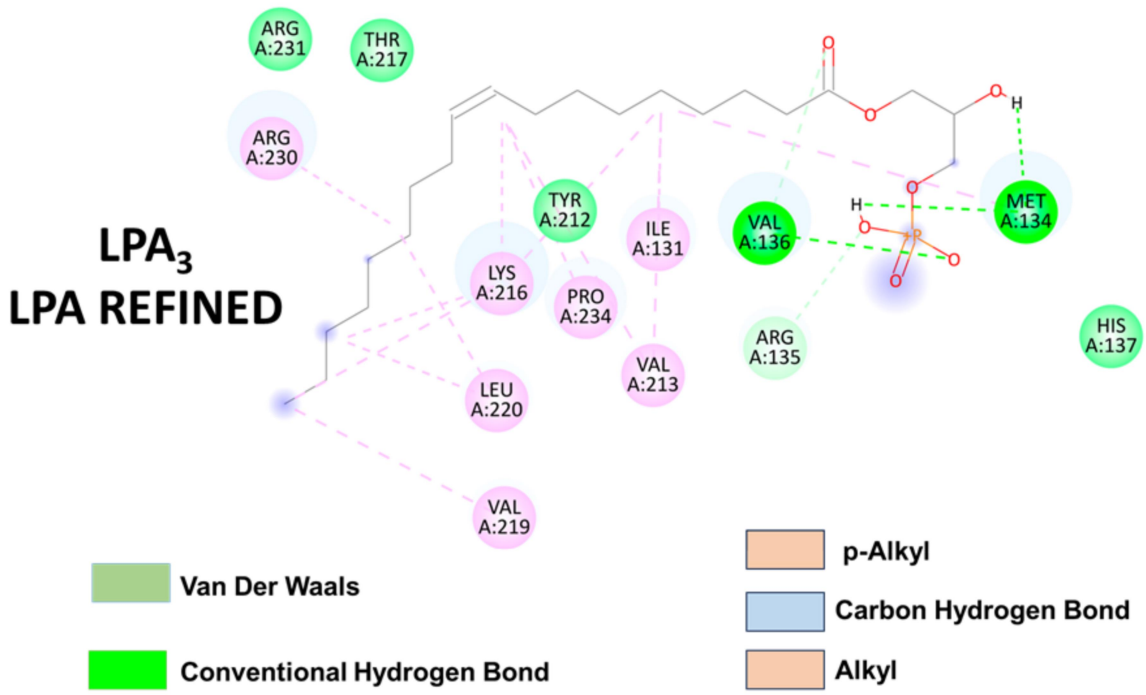

Fig. 9. The 2D diagram shows interactions at the LPA_3 binding site with OMPT (Discovery Studio Visualizer). Critical amino acids contributing to interactions are shown in circles.

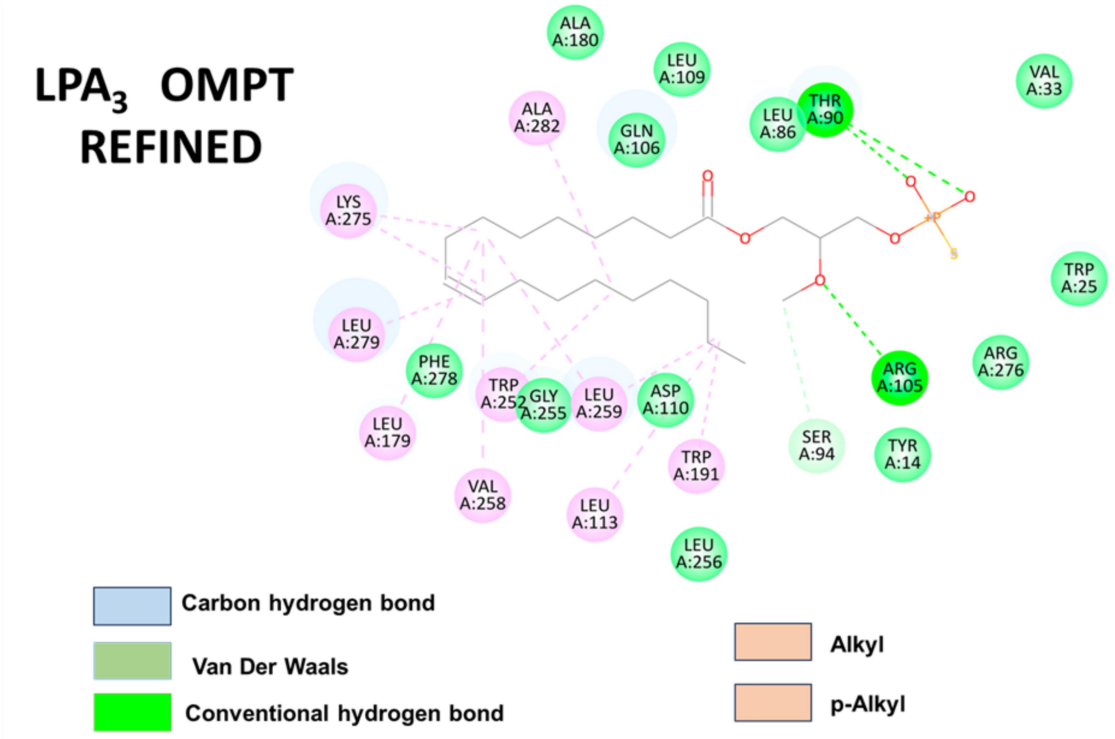

Fig. 10. Images resulting from the LPA_3-LPA (blue) and LPA_3-OMPT (red) docking analysis using PyMol

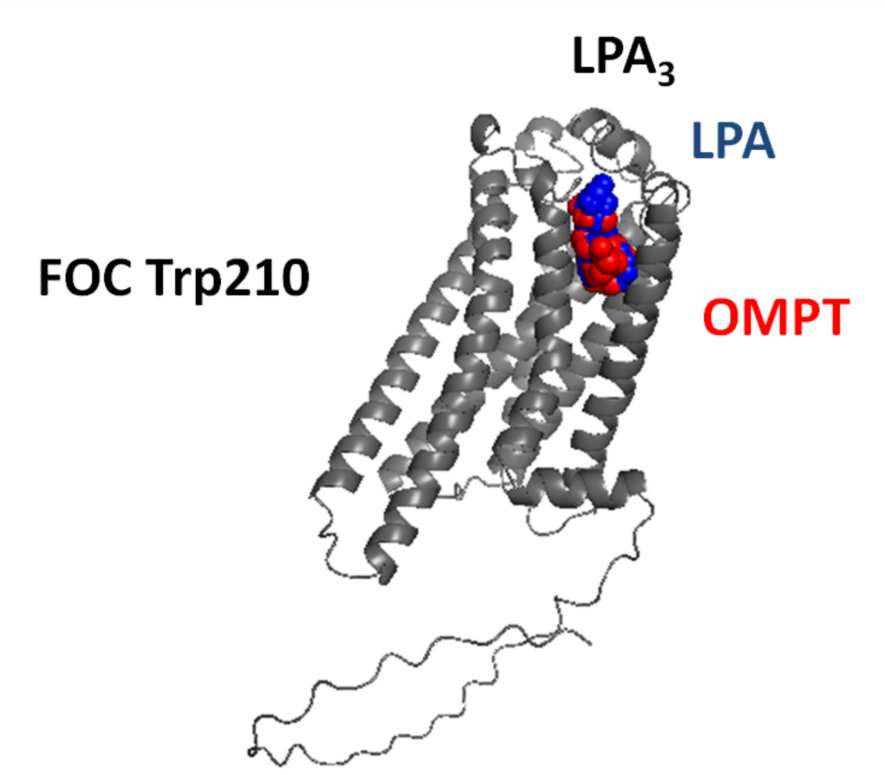

Fig. 11. Graphical representation of LPA (blue) and OMPT (red) binding to the LPA_3 receptor.

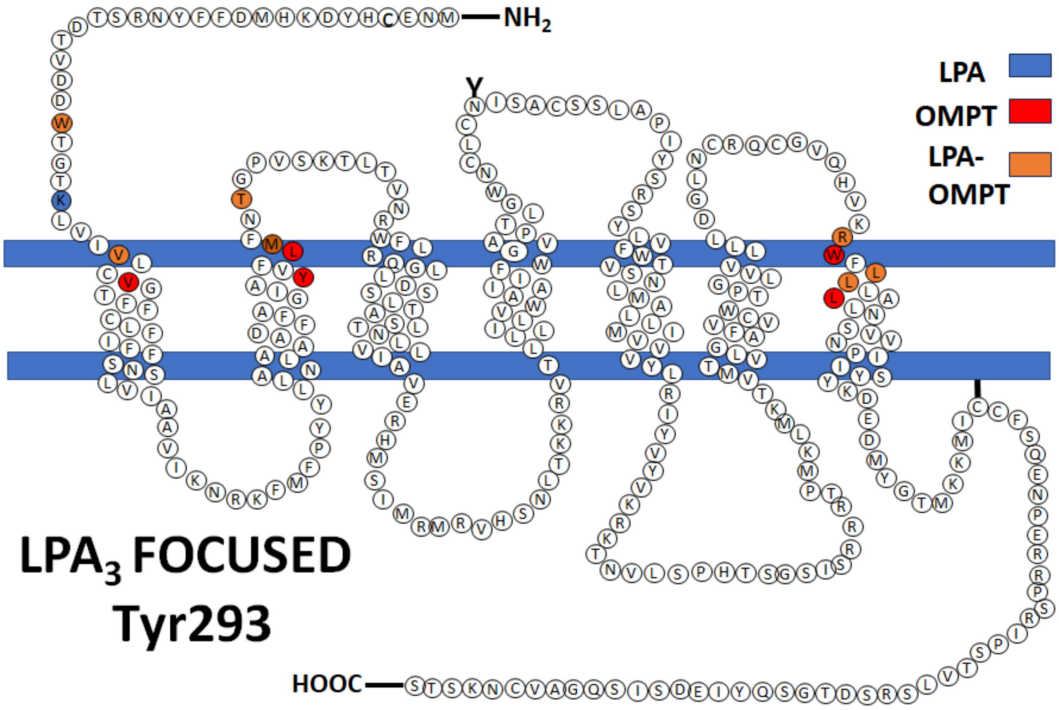

Fig. 12. The 2D diagram shows interactions at the LPA_3 binding site with LPA (Discovery Studio Visualizer). Critical amino acids contributing to interactions are shown in circles.

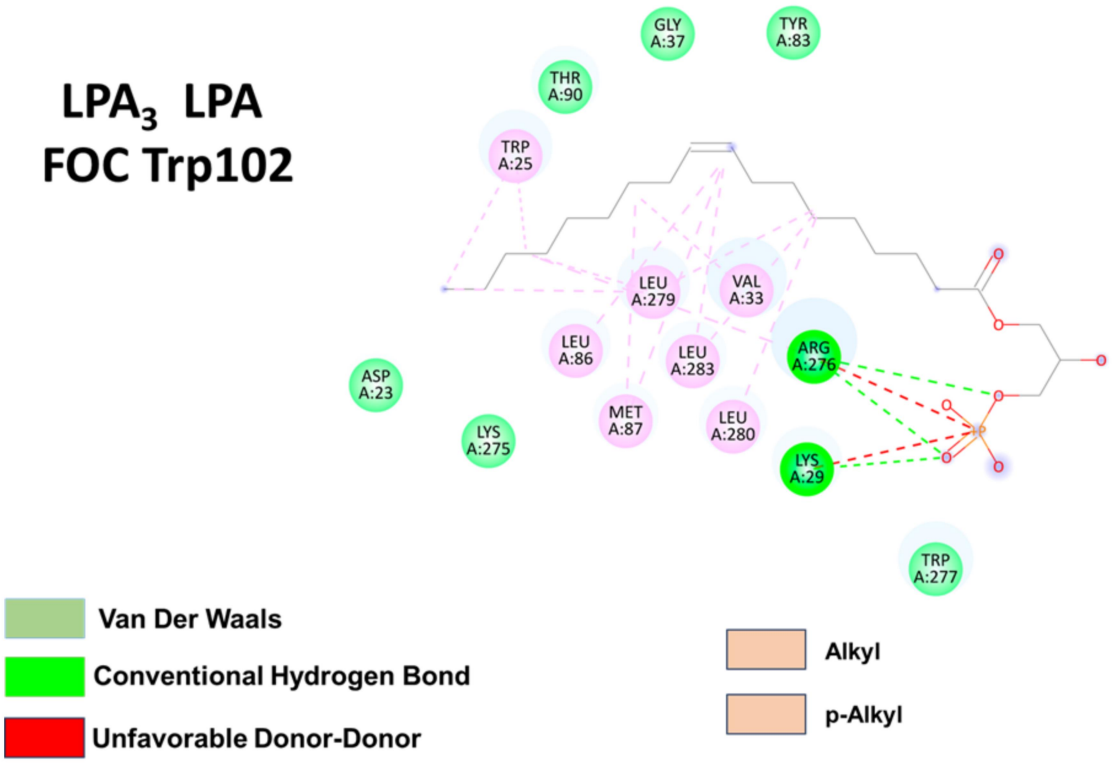

Fig. 13. The 2D diagram shows interactions at the LPA_3 binding site with OMPT (Discovery Studio Visualizer). Critical amino acids contributing to interactions are shown in circles.

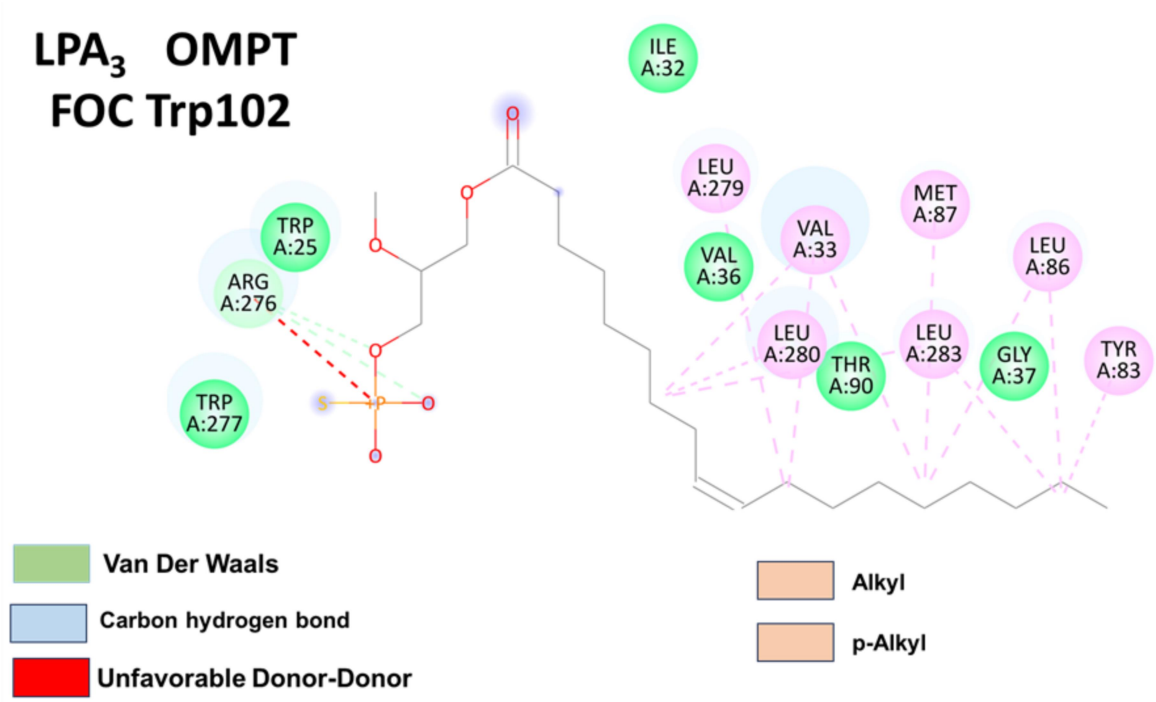

Fig. 14. Images resulting from the LPA_3-LPA (blue) and LPA_3-OMPT (red) docking analysis using PyMol

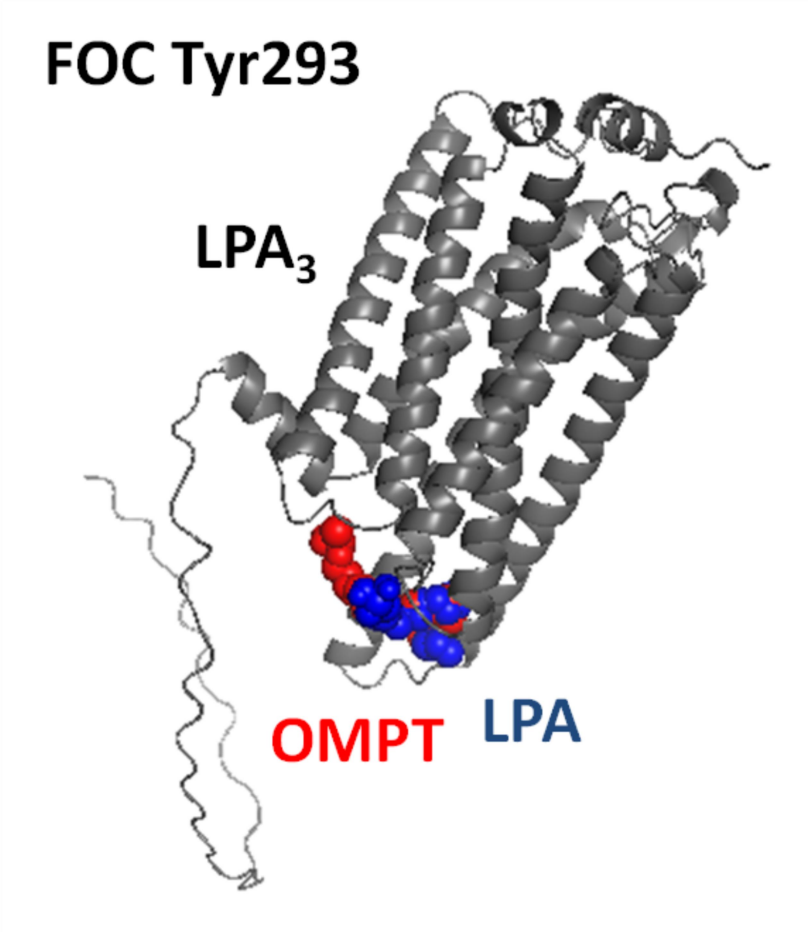

Fig. 15. Graphical representation of LPA (blue) and OMPT (red) binding to the LPA_3 receptor

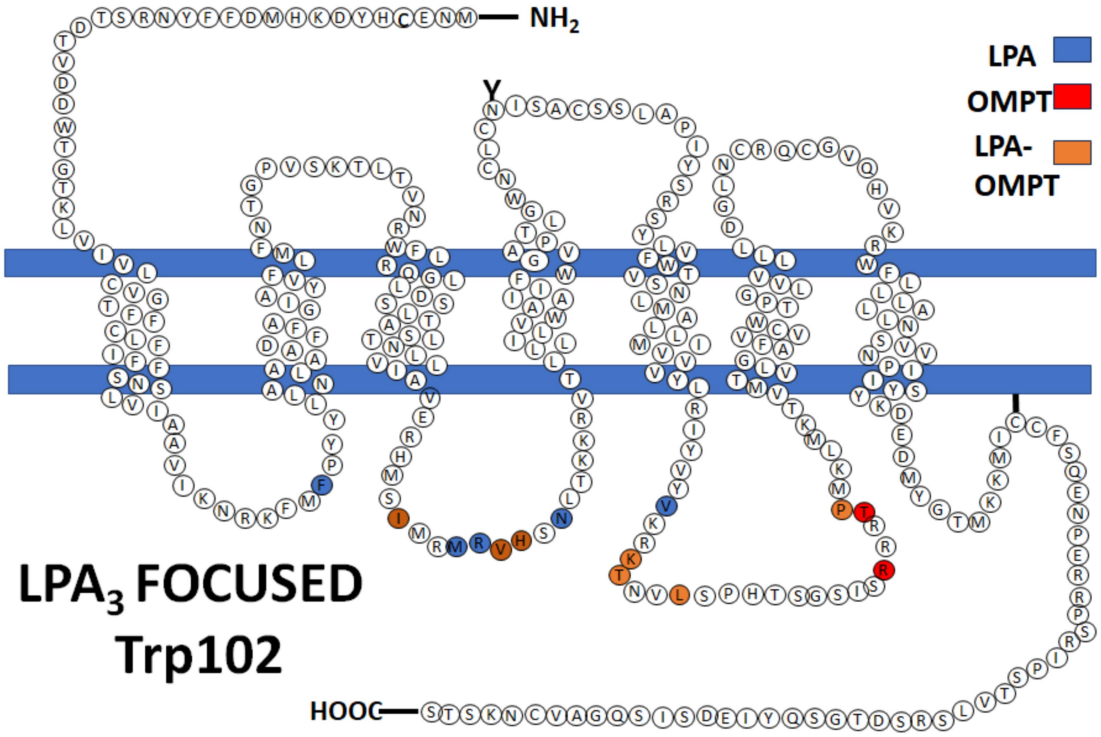

Fig. 16. The 2D diagram shows interactions at the LPA_3 binding site with LPA (Discovery Studio Visualizer). Critical amino acids contributing to interactions are shown in circles.

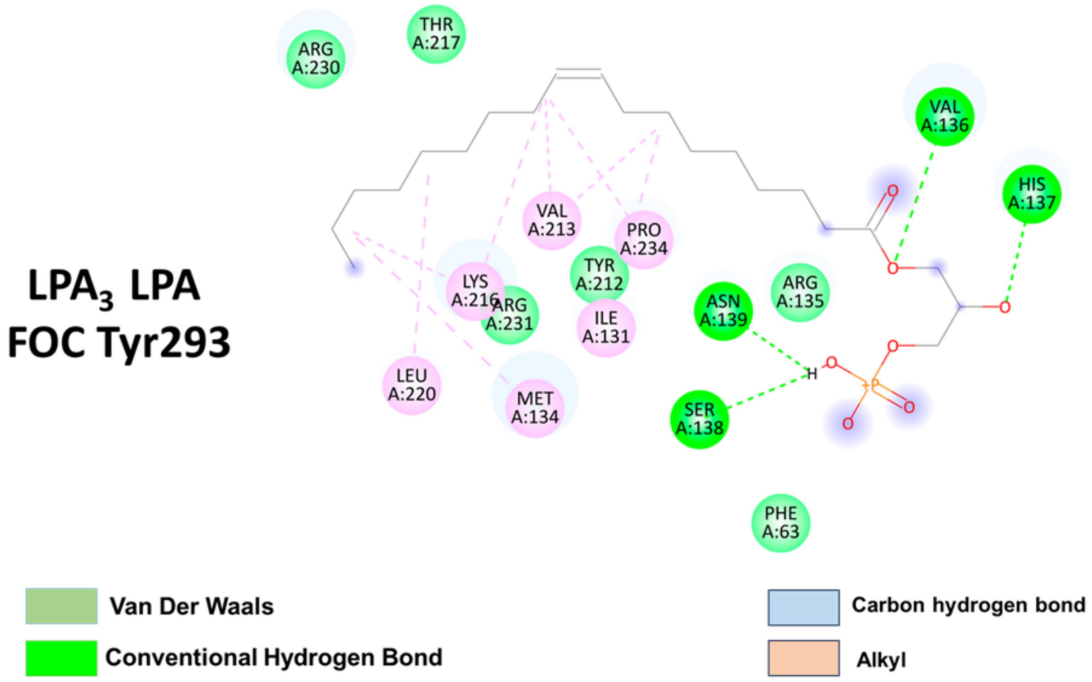
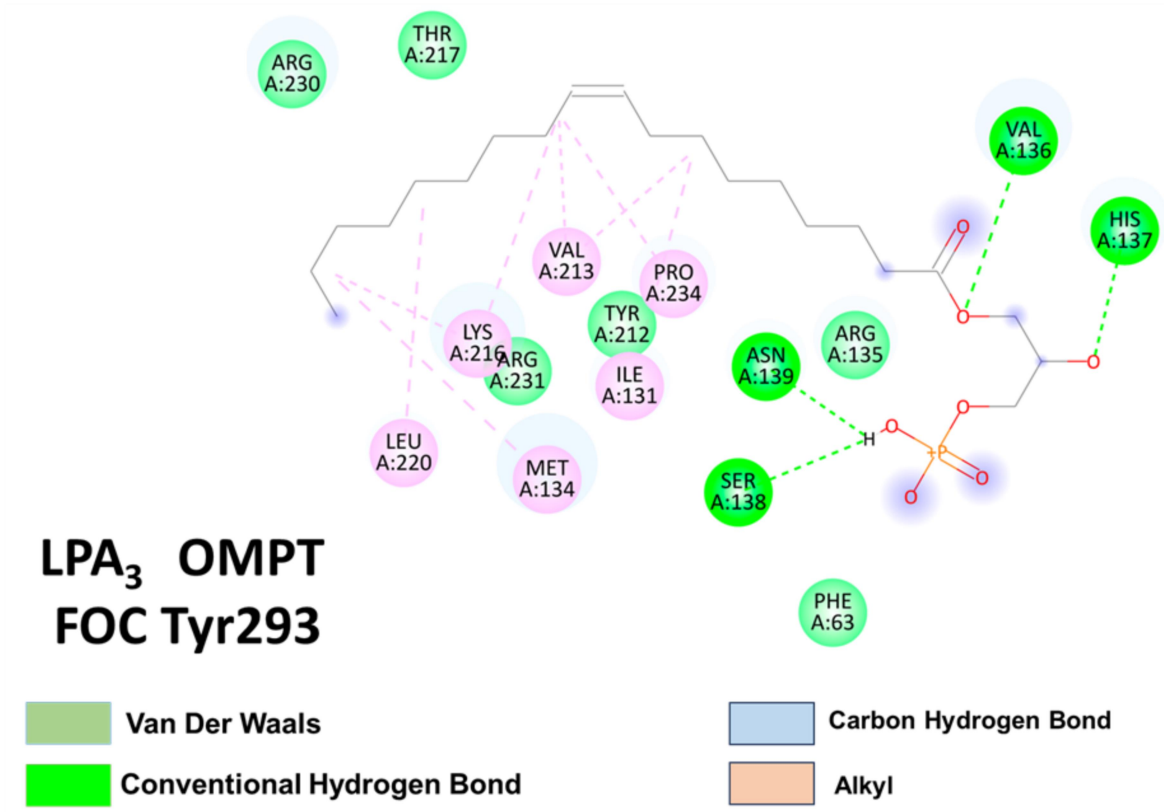
Fig. 17. The 2D diagram shows interactions at the LPA_3 binding site with OMPT (Discovery Studio Visualizer). Critical amino acids contributing to interactions are shown in circles.